Measuring simultaneously the cosmic ray composition and hadronic interaction properties

Jose Bellido

THE UNIVERSITY of ADELAIDE

The 10th International Workshop on Air Shower Detection at High Altitudes
7 - 10 January, 2020 Nanjing, P. R. China

At high energies, the cosmic ray composition is mainly determined from the depth of shower maximum (Xmax)

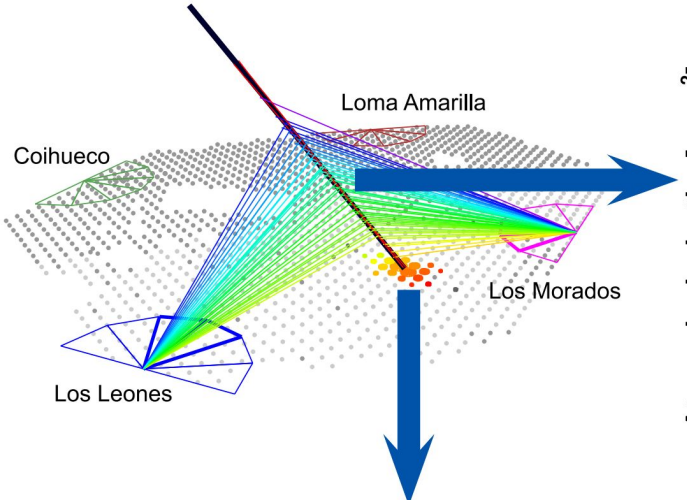

Measurement of Xmax at The Pierre Auger Observatory

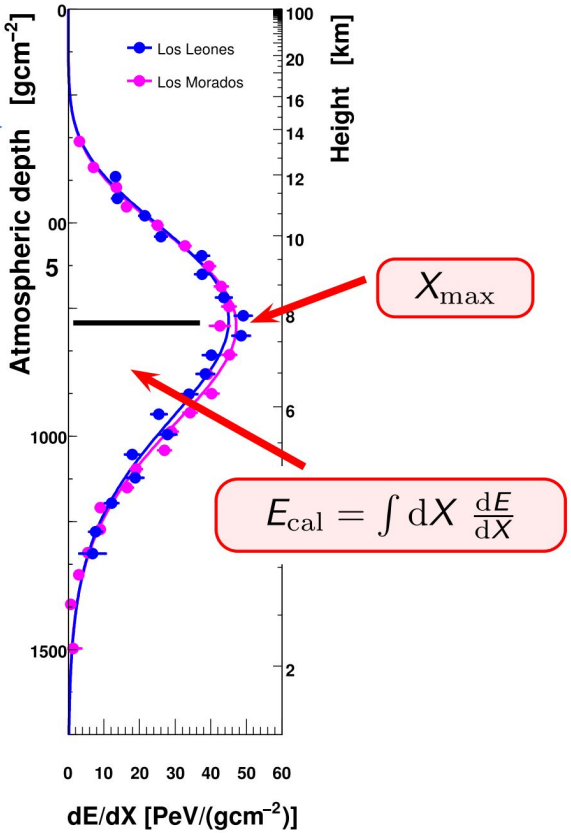

The Xmax distribution (at a given energy) is correlated with the cosmic ray composition

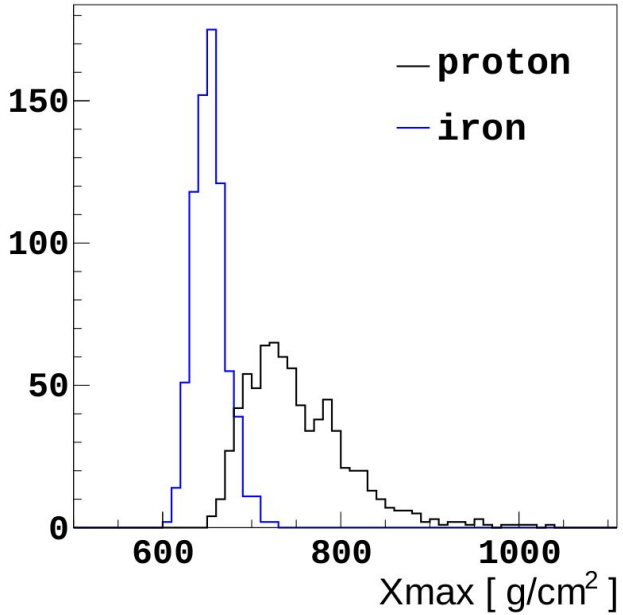

(a) An Xmax distribution of 750 proton events (black), and separately 750 iron events (blue), of energy 10^{18} eV simulated according to the EPOS-LHC hadronic interaction model.

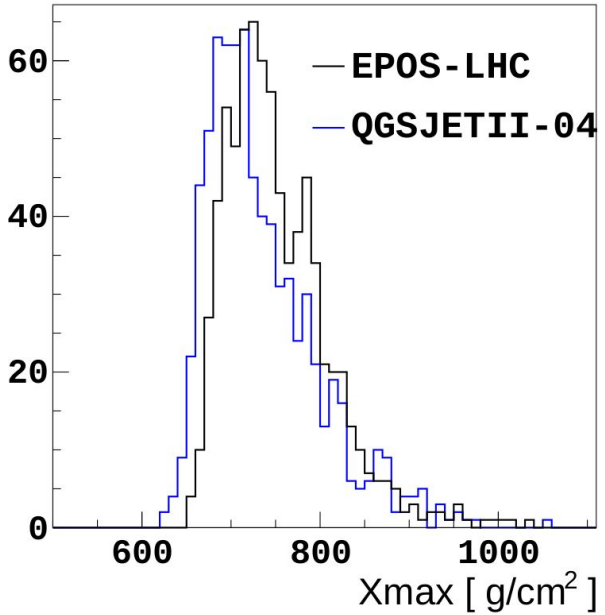

(b) An Xmax distribution of 750 EPOS-LHC simulated proton events (black), and separately 750 QGSJetII-04 simulated proton events (blue), of energy 10^{18} eV.

Pierre Auger measures X_{max} Distributions

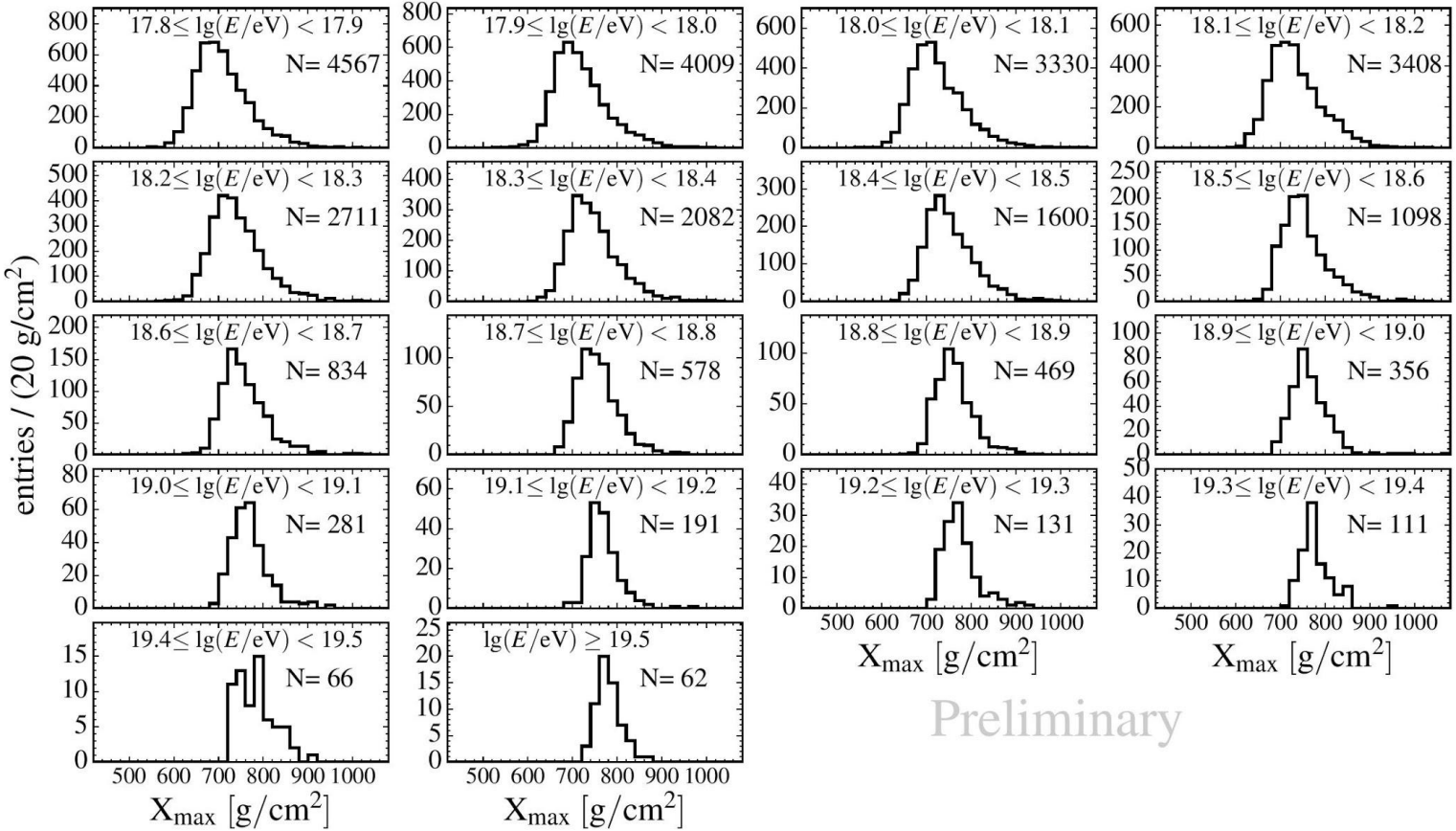

J. Bellido for the Pierre Auger Collaboration, PoS(ICRC2017)506.

Predictions from hadronic models are used to estimate the composition

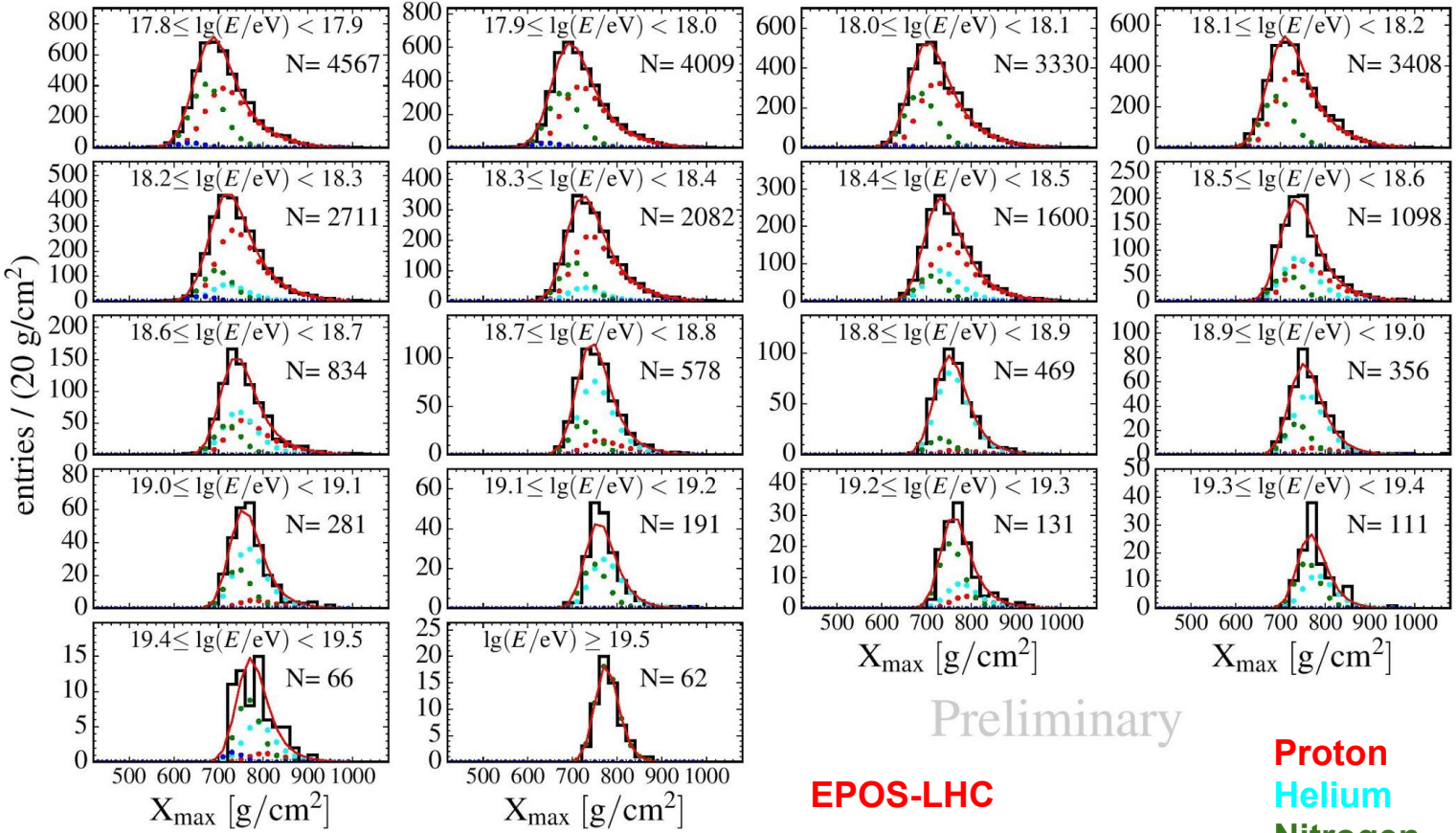

Predictions from hadronic models are used to estimate the composition

(but, different models have different X_{max} predictions and the interpretation changes significantly)

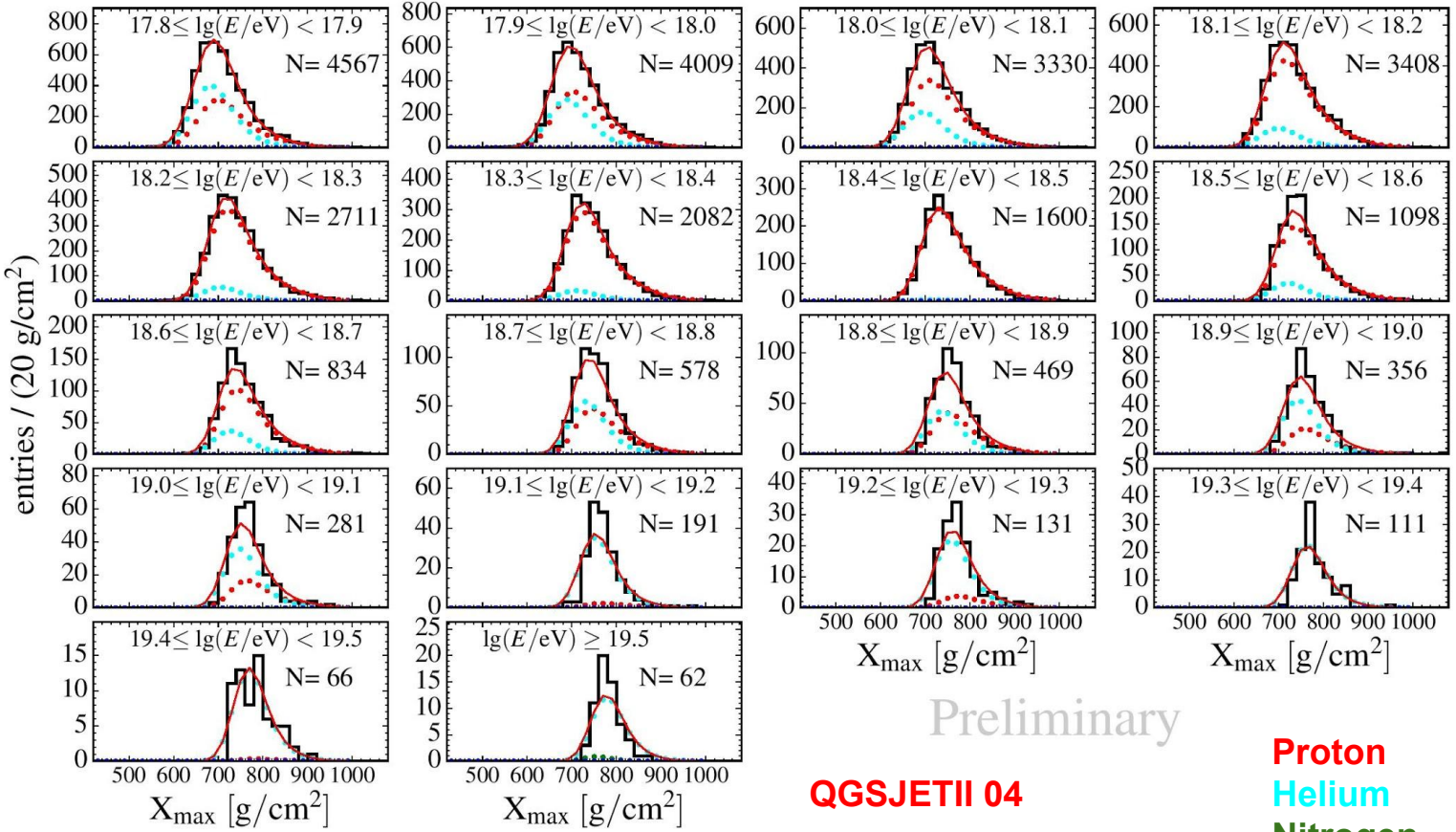

Therefore, the estimated composition is model dependent and the systematics from the models are not possible to estimate

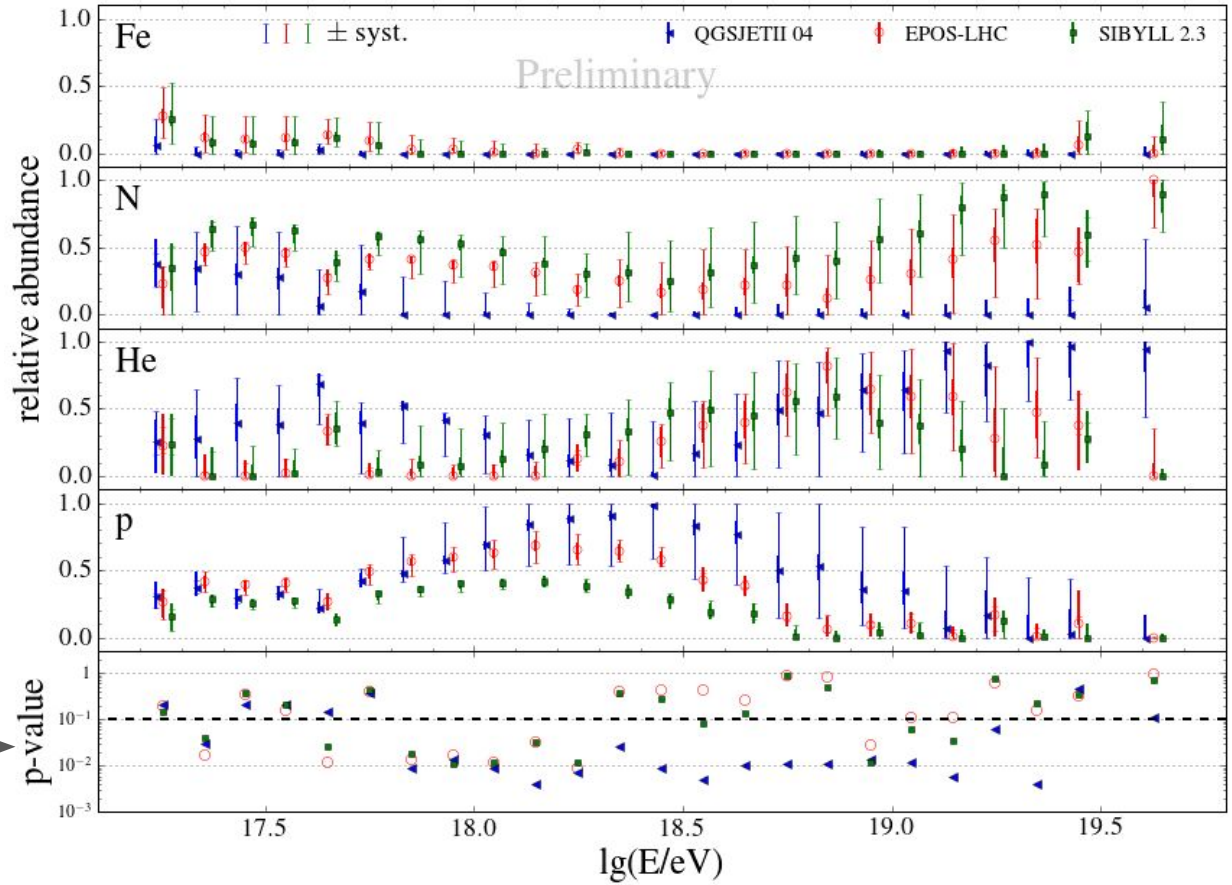

The small p-values indicate that none of the models are able to find a composition mix that is able to reproduce the observed X_{max} distributions.

J. Bellido for the Pierre Auger Collaboration, PoS(ICRC2017)506.

But, is there anything that we can say about the composition that is independent of the models?

Yes, there is!

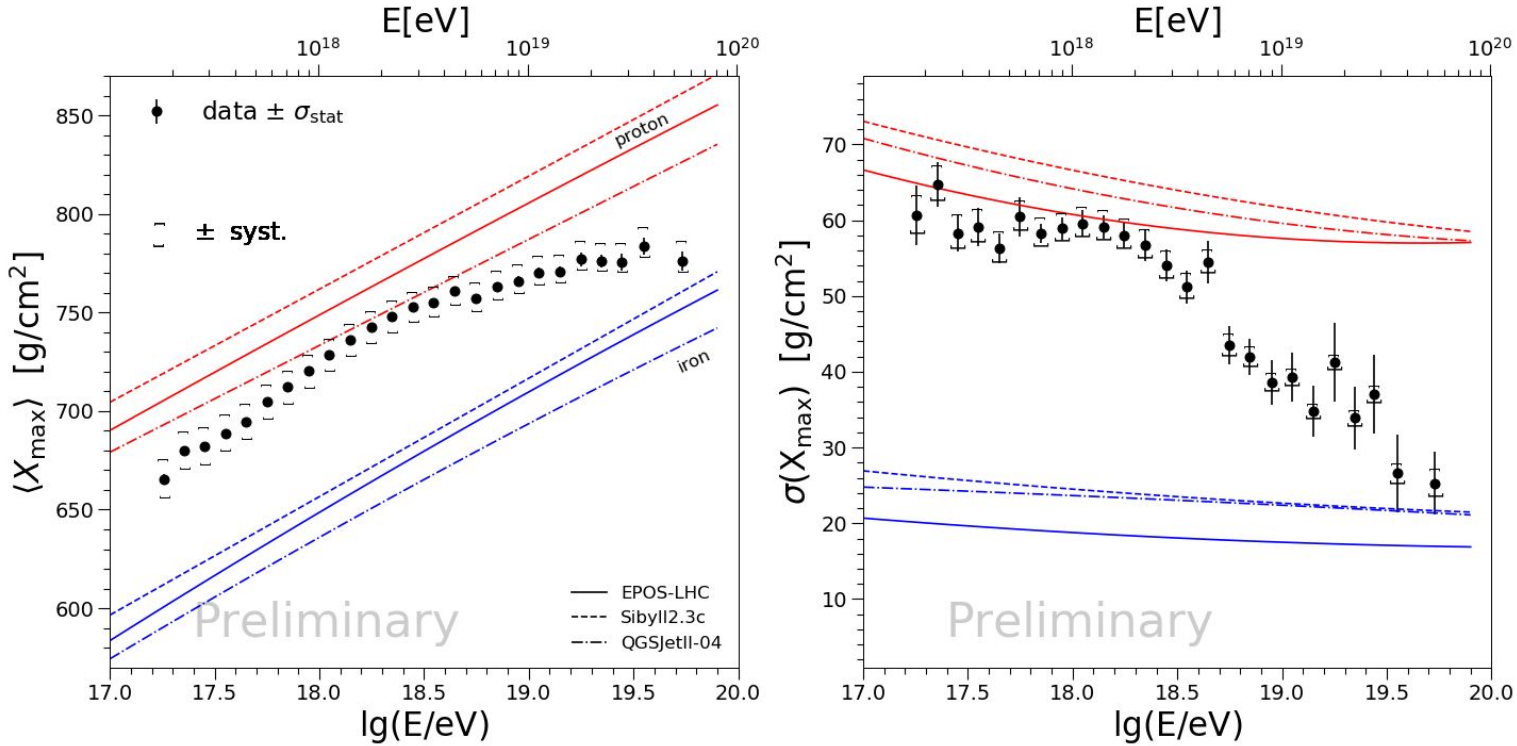

- The composition is not constant above $10^{17.2}$ eV
- It is the lightest at $10^{18.3}$ eV and gets heavier above and below $10^{18.3}$ eV

First attempt to fit simultaneously, cosmic ray composition and some model characteristics

S. Blaess, PhD thesis
The University of Adelaide

arXiv:1803.02520

a) $\langle X_{max} \rangle$ normalization is a fit parameter. However, p/Fe separation is kept constant (according to the corresponding model).

b) $\sigma(X_{max})$ normalization is a fit parameter. However, the ratio between p/Fe $\sigma(X_{max})$ is kept constant (according to the corresponding model).

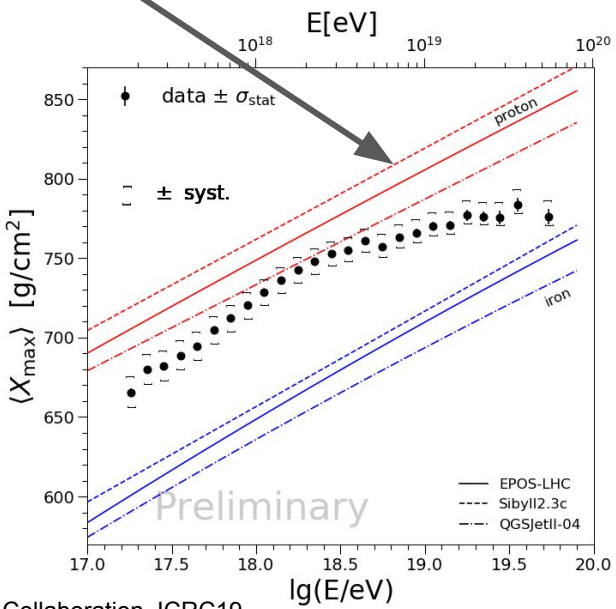

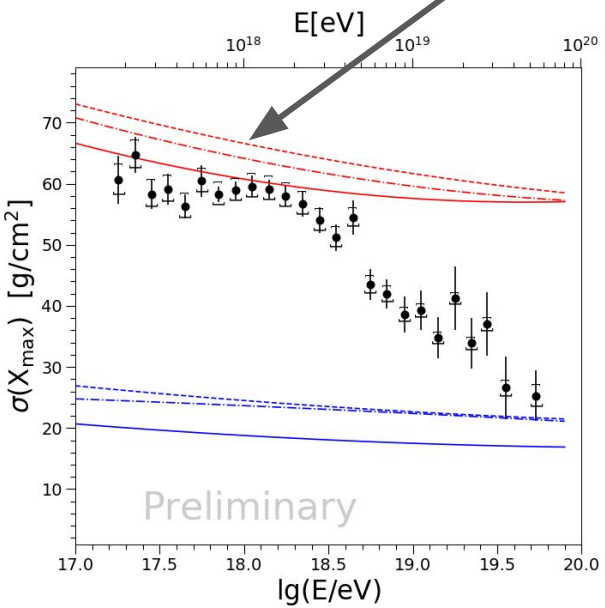

Parametrization of Xmax distribution predictions

(parameterizations are used to reduce computing time)

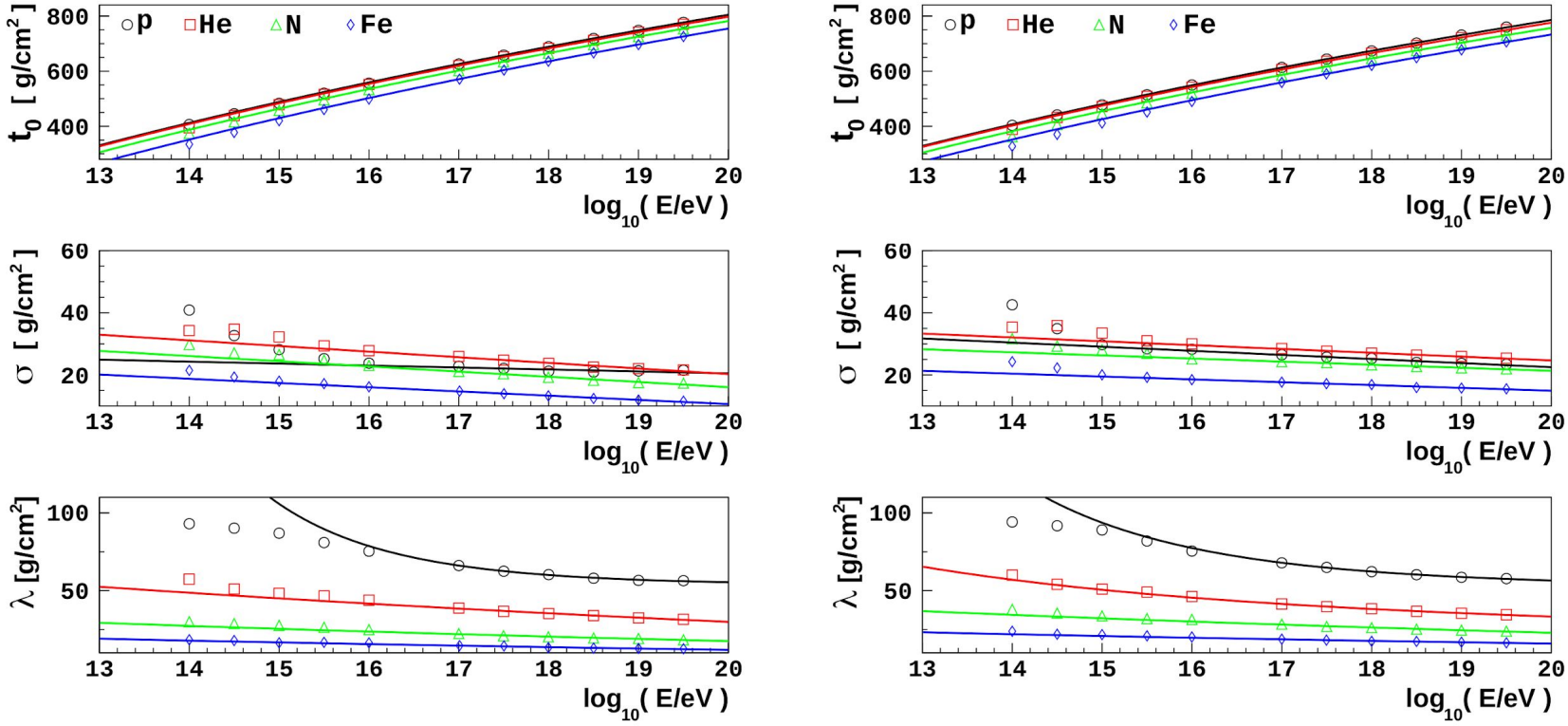

(a) EPOS-LHC

(b) QGSJetII-04

S. Blaess, PhD thesis (“Estimating composition and model properties using Xmax measurements”)
The University of Adelaide

arXiv:1803.02520

Parametrization of Xmax distributions

An $X_{\max}$ distribution of some primary energy and mass can be modelled as the convolution of a Gaussian with an exponential [238]. Three shape parameters (t_0, σ, λ) define the $X_{\max}$ distribution:

$$\frac{dN}{dX_{\max}} = \frac{1}{2\lambda} \exp\left(\frac{t_0 - t}{\lambda} + \frac{\sigma^2}{2\lambda^2}\right) Erfc\left(\frac{t_0 - t + \frac{\sigma^2}{\lambda}}{\sigma\sqrt{2}}\right), \tag{4.1}$$

where t_0 defines the mode of the Gaussian component, σ defines the width of the Gaussian component and λ defines the exponential tail of the $X_{\max}$ distribution, and t is the $X_{\max}$ bin. The mode and spread of the distribution defined in Equation (4.1) is sensitive to t_0 and σ respectively.

We fit Equation (4.1) to simulated $X_{\max}$ distributions of a particular primary energy and mass (either proton, helium, nitrogen or iron primaries) according to either the EPOS-LHC, QGSJetII-04 or Sibyll2.3 hadronic interaction model (these fits are displayed in Appendix A), obtaining the values of t_0, σ and λ for that distribution. These shape parameter (t_0, σ and λ) results are displayed in Figure 4.4, with the solid lines displaying the fits to the shape parameters as a function of energy. The functions fitted are defined as follows:

$$\begin{aligned} t_0(E) &= t_{0_{\text{norm}}} + B \cdot \log_{10}\left(\frac{\log_{10} E}{\log_{10} E_0}\right), \\ \sigma(E) &= \sigma_{\text{norm}} + C \cdot \log_{10}\left(\frac{E}{E_0}\right), \\ \lambda(E) &= \lambda_{\text{norm}} - K + K \cdot \left(\frac{\log_{10} E}{\log_{10} E_0}\right)^{\frac{L}{\ln 10}}, \end{aligned} \tag{4.2}$$

where E is the energy in eV and $E_0 = 10^{18.24}$ eV, the energy at which we choose to normalise the equations. The coefficients in Equation (4.2) are constants, and are specified in Table 4.1 for each mass component according to a particular hadronic model.

The functions of Equation (4.2) consist of two parts, the first part defining the value of a shape parameter at the normalisation energy, and the second part defining the change in the shape parameter as a function of energy. For example, $t_{0_{\text{norm}}}$ for protons would be the value of t_0 for protons at $10^{18.24}$ eV, and similarly σ_{norm} would be the value of σ at $10^{18.24}$ eV. The functions in Equation (4.2) parameterise t_0, σ and λ in Equation (4.1).

useful relations

$$\langle X_{\max} \rangle = t_0 + \lambda$$
$$\sigma(X_{\max}) = \sqrt{\sigma^2 + \lambda^2}$$

S. Blaess, PhD thesis
The University of Adelaide
arXiv:1803.02520

Evaluating the performance using mock data

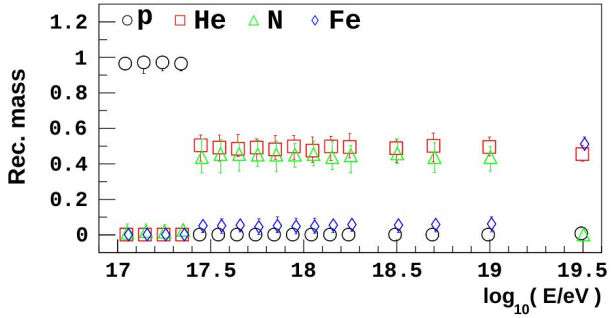

(a) QGSJetII-04 fitted to QGSJetII-04 $X_{\max}$ data.

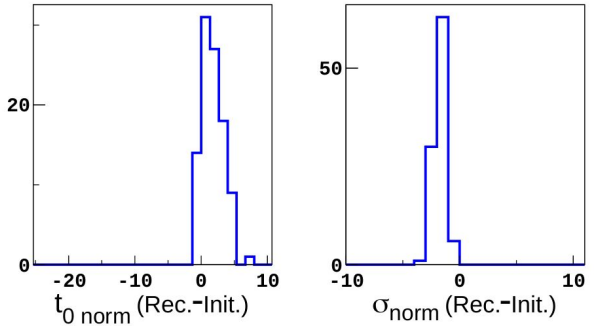

(b) Fitted coefficients from Figure 5.7a.

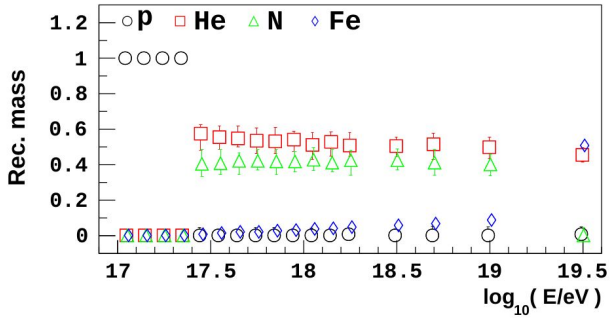

(c) EPOS-LHC fitted to QGSJetII-04 $X_{\max}$ data.

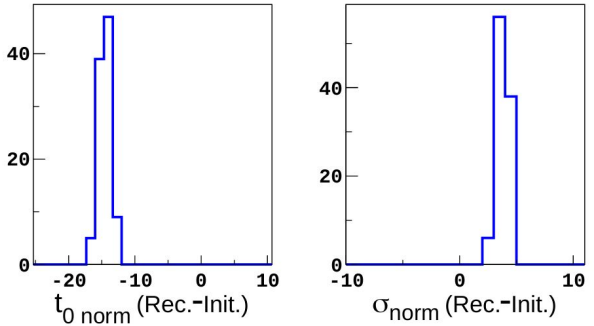

(d) Fitted coefficients from Figure 5.7c.

Figure 5.7: Fitting the mass fractions, $t_{0_{\text{norm}}}$ and σ_{norm}. The true mass composition of the data is 100% protons in the first 4 energy bins, 50% helium and nitrogen in the remaining energy bins, except the last bin which contains 50% helium and iron.

arXiv:1803.02520

Evaluating the performance using Auger-like mock data

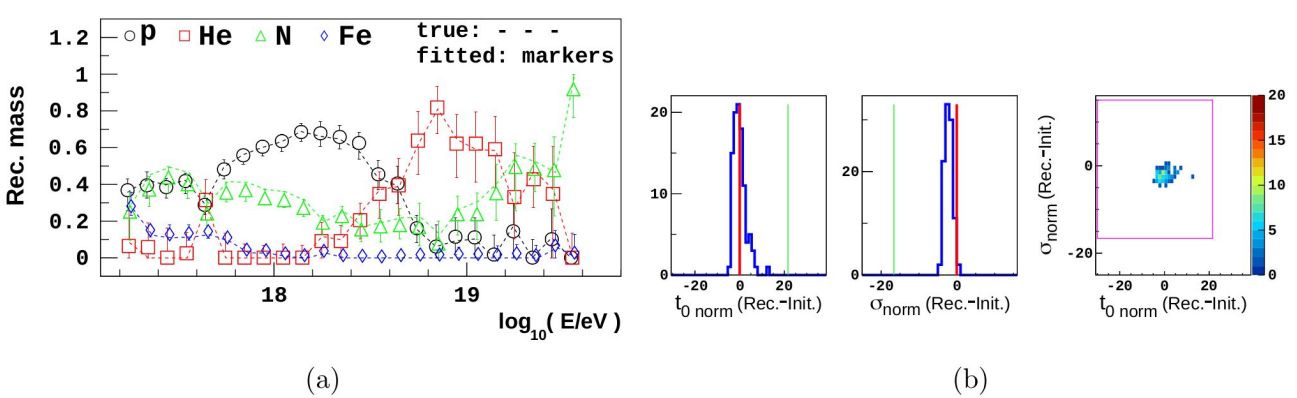

Figure 5.9: Fits of EPOS-LHC based $X_{\max}$ data with the EPOS-LHC parameterisation. See the text for an explanation of the vertical lines and the magenta boxes.

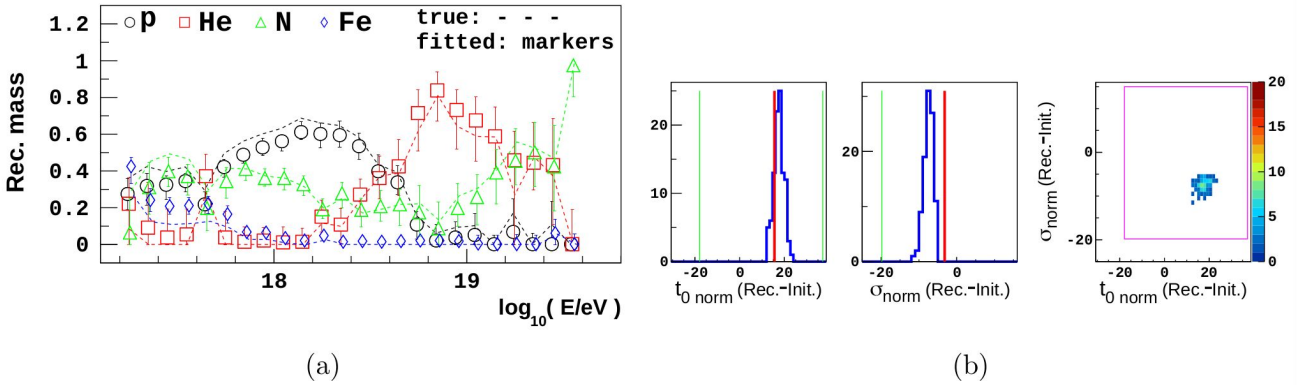

Figure 5.10: Fits of EPOS-LHC based $X_{\max}$ data with the QGSJetII-04 parameterisation.

arXiv:1803.02520

Fits to published Auger Xmax distributions for composition and normalization of $\langle X_{max} \rangle$ and $\sigma(X_{max})$

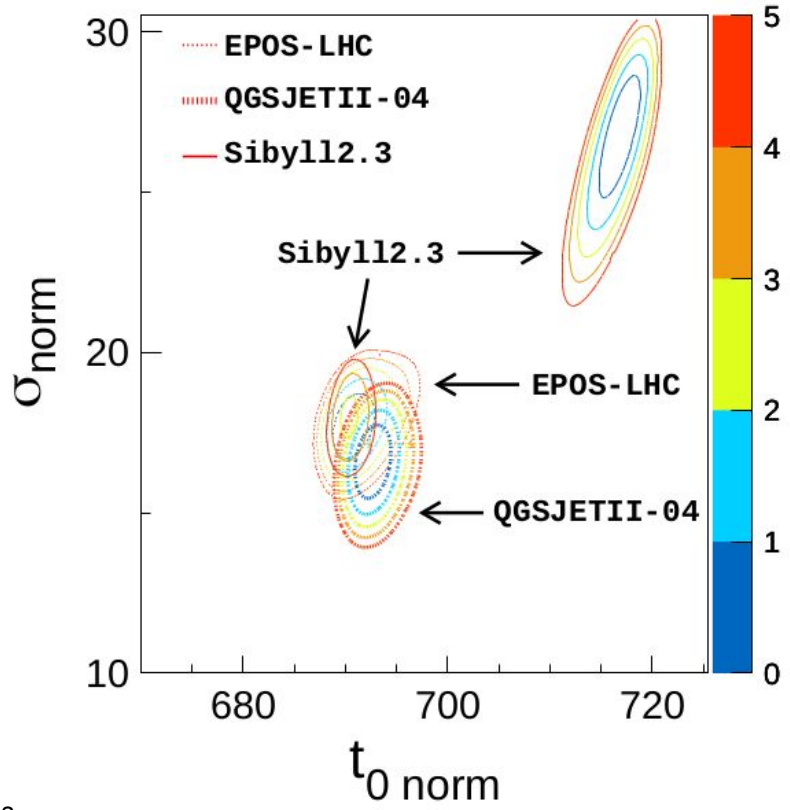

Figure 4: The $t_{0_{\mathrm{norm}}}$ and σ_{norm} parameter space scan over the Auger FD X_{max} data. For specific values of $t_{0_{\mathrm{norm}}}$ and σ_{norm} (for each model parameterisation), the mass fractions are fitted to the data, and the first 5σ contours of the minimised Poisson log likelihood ratio are shown. Notice that Sibyll2.3 has a second minimum that overlaps with the EPOS-LHC 1σ contour.

arXiv:1803.02520

Fits to Auger Xmax distributions for composition and normalization of <X_{max}> and $\sigma(X_{max})$

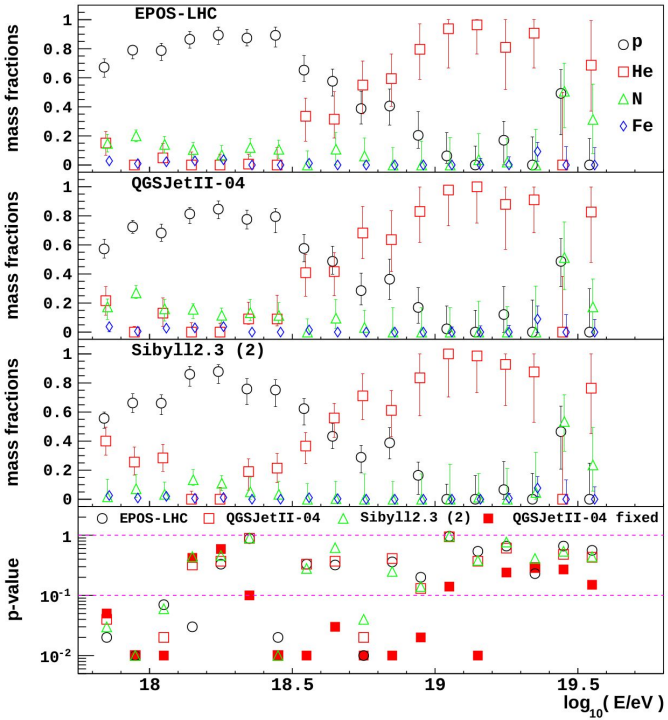

Figure 2: Fitting $t_{0_{norm}}$, σ_{norm} and the mass fractions of our parameterisations to FD X_{max} data measured by the Pierre Auger Observatory. The fitted mass fractions and p-values for each fitted model are shown. The red solid squares show the p-values (for QGSJetII-04 model) when fitting only the mass fraction ($t_{0_{norm}}$ and σ_{norm} fixed).

arXiv:1803.02520

Figure 3: The red, blue and green lines show the new predictions for the $\langle X_{max} \rangle$ and $\sigma(X_{max})$ after fits of $t_{0_{norm}}$, σ_{norm} and the mass fractions to FD X_{max} distributions measured by the Pierre Auger Observatory.

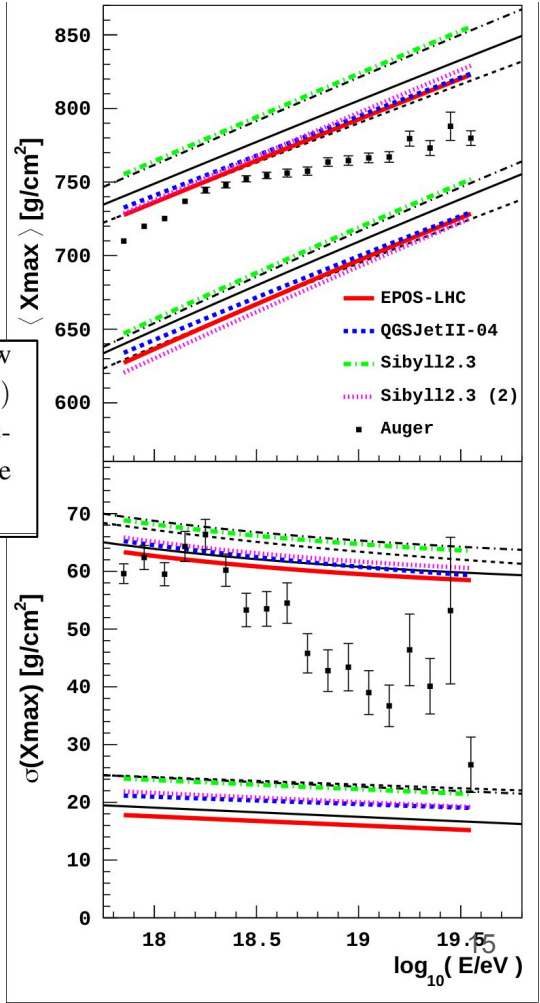

Fits to Auger Xmax distributions for composition and normalization of $\langle X_{max} \rangle$ and $\sigma(X_{max})$

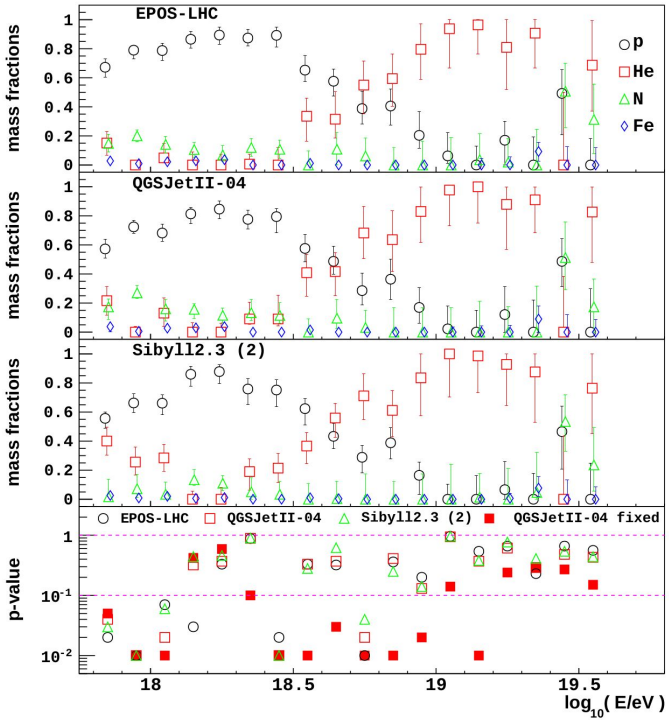

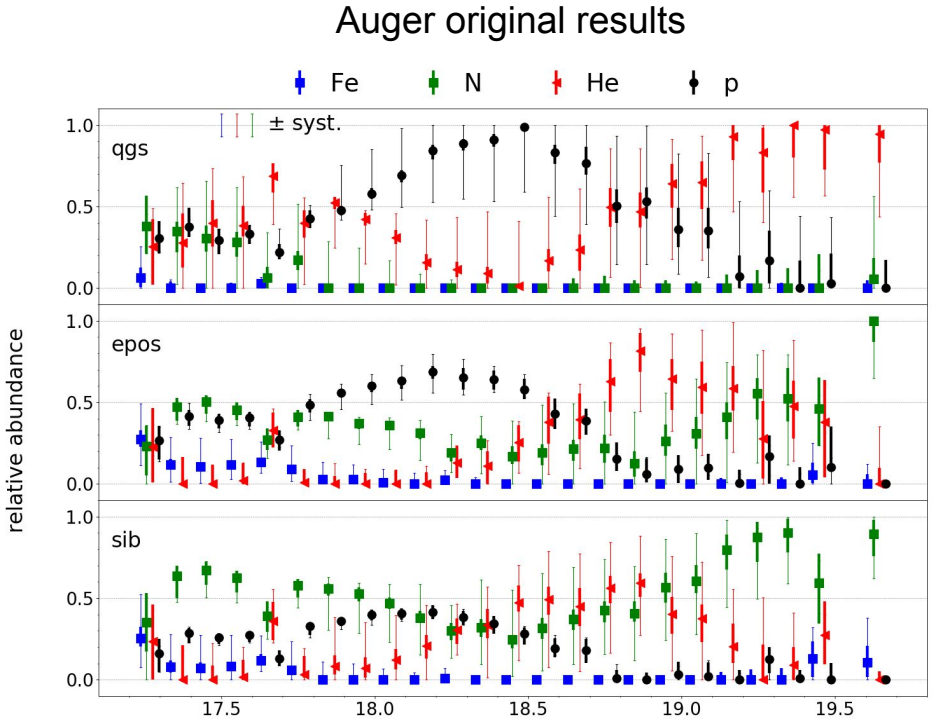

Figure 2: Fitting $t_{0_{\rm norm}}$, $\sigma_{\rm norm}$ and the mass fractions of our parameterisations to FD $X_{\rm max}$ data measured by the Pierre Auger Observatory. The fitted mass fractions and p-values for each fitted model are shown. The red solid squares show the p-values (for QGSJetII-04 model) when fitting only the mass fraction ($t_{0_{\rm norm}}$ and $\sigma_{\rm norm}$ fixed).

Following steps ...

- **Include other shower observables**, such as number of muons, electromagnetic signal, or ratio of muonic/electromagnetic signals.

- **Include** measurements from **different experiments** (i.e. **LHAASO**, IceCube, Auger) covering a wider energy range (from TeV up to around 10^{20} eV) and sampling the air shower at different atmospheric depths.

- **Bootstrap models and composition**. Instead of using parametrizations for model predictions (to be compared with the data), models would be modified (tuned) and their new predictions (for different cosmic ray compositions) would be compared with observations from different experiments. We hope to find a new set of model properties (and composition as a function of energy) that make possible a coherent description of all observables from at all experiments. **This process requires high computing power!**

Conceptual framework

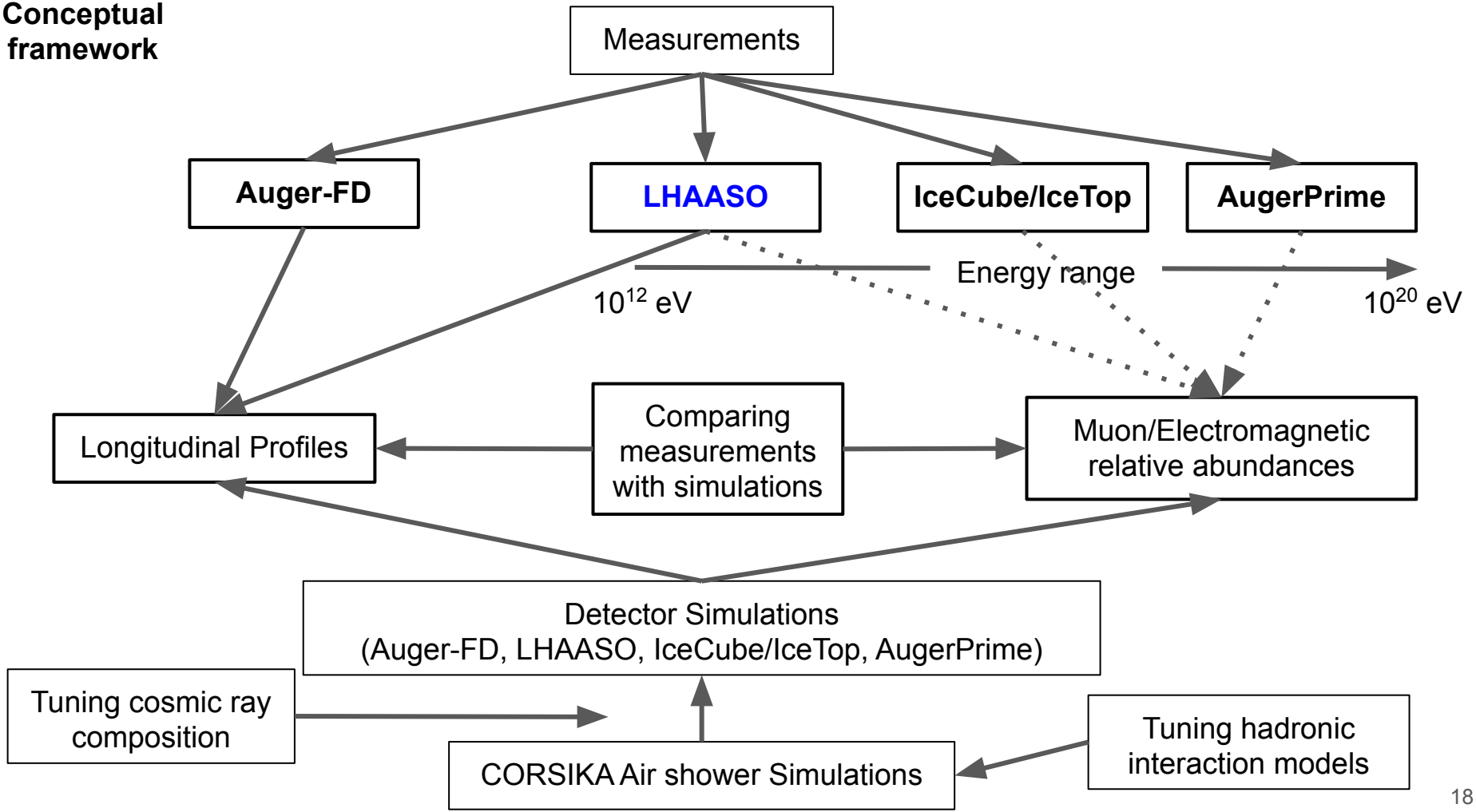

https://gambit.hepforge.org/

Introducing GAMBIT

GAMBIT is a global fitting code for generic Beyond the Standard Model theories, designed to allow fast and easy definition of new models, observables, likelihoods, scanners and backend physics codes.

GAMBIT: The Global And Modular BSM Inference Tool

- Fast definition of new datasets and theoretical models
- Plug and play scanning, physics and likelihood packages
- Extensive model database – not just SUSY
- Extensive observable/data libraries
- Many statistical and scanning options (Bayesian & frequentist)
- *Fast* LHC likelihood calculator
- Massively parallel
- Fully open-source

ATLAS	A. Buckley, P. Jackson, C. Rogan, M. White,
LHCb	M. Chrząszcz, N. Serra
Belle-II	F. Bernlochner, P. Jackson
Fermi-LAT	J. Conrad, J. Edsjö, G. Martinez, P. Scott
CTA	C. Balázs, T. Bringmann, J. Conrad, M. White
HESS	J. Conrad
IceCube	J. Edsjö, P. Scott
XENON/DARWIN	J. Conrad, R. Trotta
Theory	P. Athron, C. Balázs, T. Bringmann, J. Cornell, J. Edsjö, B. Farmer, T. Gonzalo, S. Hoof, F. Kahlhoefer, A. Krislock, A. Kvellestad, M. Pato, F. Mahmoudi, J. McKay, A. Raklev, R. Ruiz, P. Scott, R. Trotta, C. Weniger, M. White

Co-spokesperson and is also based at the University of Adelaide

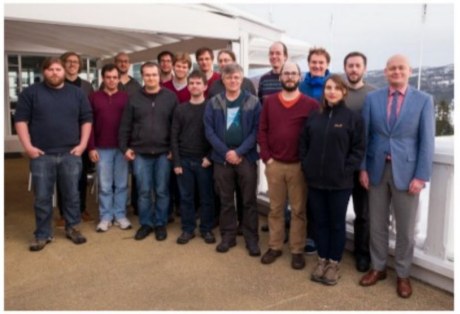

27 Members, 9 Experiments, 4 major theory codes, 10 countries

Summary

- Significant efforts are required to understand the physics of high energy showers. Which is critical for interpret air shower observations in terms of the cosmic ray mass composition.

- It is necessary to combine observations from different experiments such as **LHAASO**, IceCube and Auger to constraint high energy hadronic models. These observations will constraint different aspects of the models over a wider energy range, and at different stages of the shower development (i.e. the ground arrays are at different altitudes).

The difference between model predictions persists despite recent measurements at the LHC

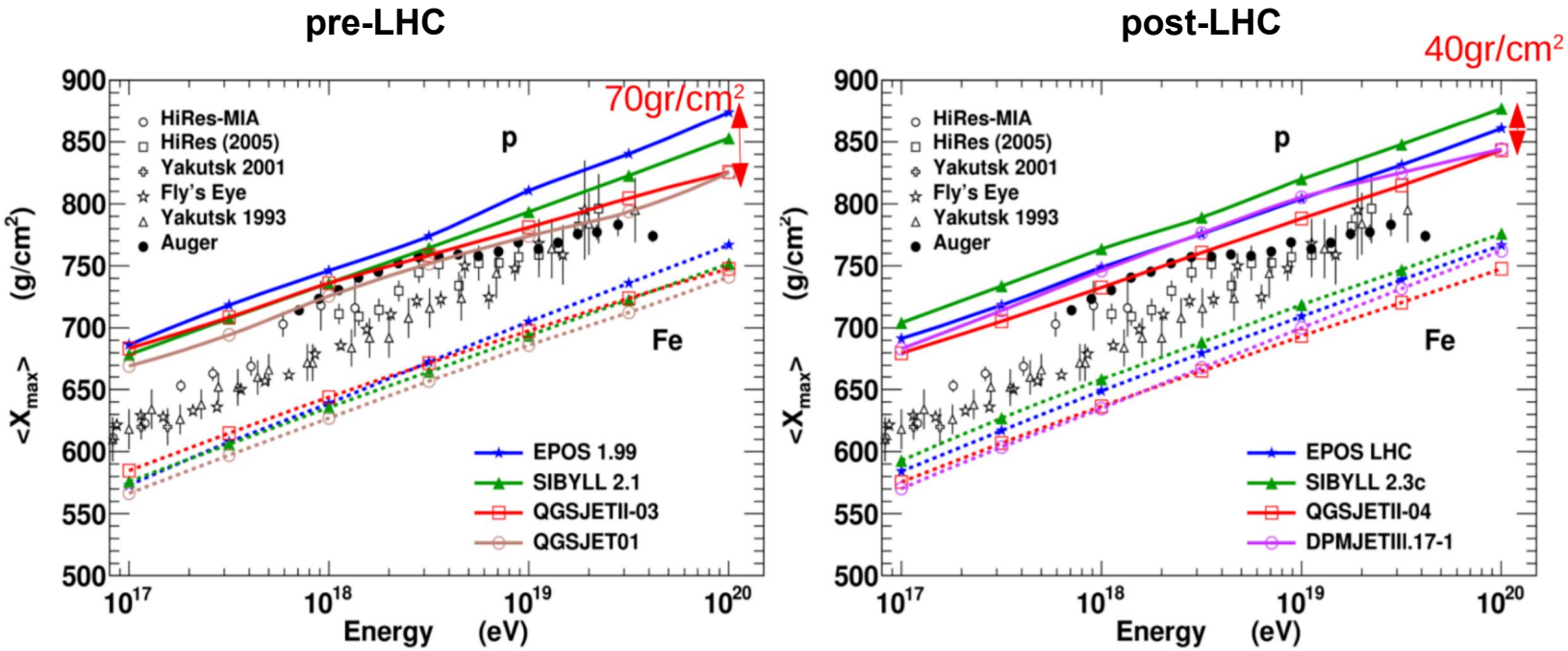

T. Pierog. ICRC 2017.